Precipitation teleconnections during 1950-2021 over the Arabian Peninsula

Matthew F. Horan[1,2] Nathaniel C. Johnson[3] Fred Kucharski[4], Muhammad Adnan Abid[4], Sarah B. Kapnick[5], Moetasim Ashfaq[1,2]

[1] Computational Sciences and Engineering Division, Oak Ridge National Laboratory, Oak Ridge, Tennessee, United States

[2] Bredesen Center, University of Tennessee, Knoxville, Tennessee, United States

[3] Geophysical Fluid Dynamics Laboratory, National Oceanic and Atmospheric Administration, Princeton, NJ, United States

[4] Section of Earth System Physics, Abdus Salam International Centre for Theoretical Physics, Trieste, Italy

[5] National Oceanic Atmospheric Administration, Washington, DC, United States

Corresponding author: Matthew Horan (mhoran@vols.utk.edu)

Key Points:

- Global patterns associated with Arabian Peninsula (AP) precipitation display substatial differences between winter and spring months.
- Several global teleconnections' correlation with precipitation variability over the AP displayed a drastic shift in the 1980s.
- El Niño-Southern Oscillation diversity and indirect influence is a key factor in fully understanding AP precipitation variability.

Abstract

This study investigates precipitation variability over the Arabian Peninsula (AP) during its wet season. The wet season is split into winter (November – February) and spring (March and April) seasons, and early (1950–1986) and late (1986–2021) periods to understand sub-seasonal characteristics of precipitation variability and long-term changes in global teleconnections. The first three Empirical Orthogonal Functions explain ~70% of the interannual wet season precipitation variance, which shows an increase (decrease) in the late period winter (spring). Linear regression of the sea surface temperatures and geopotential height onto associated principal components reveals many oceanic and atmospheric variability patterns, which exhibit significant differences between winter and spring and early and late periods. Further, linear regressions of AP precipitation onto 14 natural modes of climate variability reveal a complex network of global teleconnections. El Niño-Southern Oscillation (ENSO) is one of the key contributors to precipitation variability but considering ENSO diversity is crucial to fully understand its influence. While the direct ENSO influence only becomes robust after the 1980s, its indirect effect persists through projection onto atmospheric modes, such as East Atlantic West Russia Pattern and East Atlantic Mode, or inter-basin interaction (e.g., via the Indian Ocean). The Northern Hemisphere atmospheric modes also mediate influences of other natural modes in tropical Indian and Atlantic oceans and extra-tropical regions over the AP. Several precipitation teleconnections exhibit a shift in the 1980s. Some may be related to the introduction of satellite data, but further investigations are warranted to understand the causes of these shifts.

Plain Language Summary

The Arabian Peninsula (AP) receives very little precipitation and accurate prediction of that precipitation is vital for socioeconomic planning in the region. Most of the precipitation that does occur occurs between November and April, known as the wet season. We analyze the main patterns of how precipitation changes over the Arabian Peninsula. We additionaly analyze how 14 global height, pressure, and sea surface temperature patterns and three definitions of the El Niño-Southern Oscillation (ENSO) using different regions of sea surface tempeatures are correlated with precipitation over the Arabian Peninsula. Through this analysis, while we find that a lack of data makes results questionable in the southern portions of the AP, there is a distinct change in the most prominent patterns between the wintner months (November – February) and the spring months (March-April). We additionally find that the region of the Pacific Ocean used to define ENSO is important in determining it's association with AP precipitation. While a direct influence of ENSO and several other patterns is only evident after a major shift in many patterns' correlation in the 1980s, evidence of ENSO's projection onto other patterns more consistently correlated with AP precipitation are present throughout the time period.

1 Introduction

The Arabian Peninsula (AP) is an arid to semi-arid region of the world with most low-lying areas having an annual precipitation of less than 150 mm and higher elevations averaging about 300 mm per year of precipitation (Almazroui et al., 2012; Almazroui, 2011; Edgell, 2006; Abdullah & Al-Mazroui, 1998; Almazroui et al., 2013). AP precipitation is highly variable, and its accurate prediction is vital for informed water resources and socioeconomic planning. With limited freshwater resources and a rapidly warming regional climate that regularly reaches

extreme temperatures due to the background environmental conditions, knowing the changes in the likelihood of anomalously wet and dry years is critical for the region. Trends since 1980 indicate drying patterns with decreasing precipitation reaching statistical significance over the central AP (Kwarteng et al., 2009; Almazroui et al., 2012; Alsaaran & Alghamdi, 2022; Syed et al., 2022; Horan et al., 2022).

In most areas of AP, over 90% of the annual precipitation falls between November and April (Almazroui, 2011; Abdullah & Al-Mazroui, 1998), a period known as the wet season. The precipitation distribution exhibits spatial heterogeneity, with higher magnitudes limited to the northern AP, central Saudi Arabia, and the coastal areas through Oman. The exception is the areas bordering the Red Sea that are influenced by topographic-induced convection and receive noticeable precipitation (~30 %) outside the wet season (Horan et al., 2022). Several studies project that a continuously warming climate may lead to more commonplace occurrences of extreme precipitation and prolonged droughts across the AP region (Almazroui & Saeed, 2020; Donat et al., 2014). The aridity of AP climate, high seasonality of received precipitation, and vulnerability to future climate change highlight the need for reliable seasonal predictions and long-term climate projections. To this end, noting the relative roles of natural climate variability and anthropogenically driven climate change in shaping the characteristics of AP climate is essential for resource planning at varying timescales.

The natural modes of climate associated with sea surface temperature (SST) anomalies in the tropical oceans and internal atmospheric variability in the Northern Hemispheric have been known to have a role in inter-annual precipitation variability across the region during the wet season (e.g., Mehmood et al., 2022; Alamzroui et al., 2013; Donat et al., 2014; Kang et al., 2015; Abid et al., 2016). The most well-known and widely studied phenomenon with influence over the AP is the El Niño-Southern Oscillation (ENSO). Studies show that the positive (negative) phase of ENSO is related to an increase (decrease) in precipitation over most of the AP (Almazroui et al., 2013; Donat et al., 2014; Kang et al., 2015; Atif et al., 2020; Horan et al., 2022; Abid et al., 2016, 2020). Kang et al. (2015) additionally noted the strengthening of ENSO influence on AP precipitation in recent decades. Moreover, other studies on the Saudi Arabian climate relate the positive phase of the Indian Ocean Dipole (IOD; Saji et al., 1999) with more wet events (Chakraborty et al., 2006), while the negative phase of the Pacific Decadal Oscillation (PDO, Mantua et al., 1997) with an increase in the likelihood of droughts (Syed et al., 2022). However, much of this research is focused on the last 3-4 decades, and long-term variability in these teleconnections is not fully known.

Moreover, there has been little research regarding the potential role of Atlantic Ocean SST variability on precipitation over the AP. Likewise, robust knowledge of the influences exerted by the internal modes of variability in the Northern Hemisphere is also lacking. The North Atlantic Oscillation (NAO) – the most prominent mode of variability in the Northern Hemisphere during winter – has been shown to have a generally negative, though statistically insignificant correlation with precipitation over most of the AP (Saeed & Almazroui, 2019; Ehsan et al., 2017; Atif et al., 2020; Donat et al., 2014; Horan et al., 2022). However, several other frequently occurring Northern Hemisphere atmospheric patterns (Barnston & Livezey 1987), such as East Atlantic Mode (EAM), East Atlantic West Russia Pattern (EAWR), and Siberian High (SH), may

also impact AP precipitation through the modulation of extratropical storm tracks, which warrants thorough investigation.

Given the highlighted gaps in our understanding, this study systematically investigates the potential influences of 14 naturally occurring modes of oceanic and atmospheric variability on AP precipitation since the mid of the 20th century, and how they relate to the most common variations of precipitation over the Arabian Peninsula. A more extended analysis period allows the identification of any shifts that might have occurred in remote teleconnections. Moreover, the nature of these teleconnections has been investigated separately for the early (November to February) and late (March–April) wet seasons to understand their intra-seasonal persistence or variations. Section 2 discusses the data, methods, and indices used throughout this study. Section 3 provides an overview of the analysis and results, further discussed in section 4. Finally, section 5 summarizes the main findings and discusses future directions to improve understanding of AP climate.

2 Data and Methods

2.1. Data used

Our analysis uses monthly mean total precipitation, 500 hPa geopotential height (GPH), mean sea level pressure (SLP), and sea surface temperature (SST) variables from the European Centre for Medium Range Weather Forecast's fifth generation reanalysis (ERA5) with complete data from 1959 to 2021 (Hersbach et al., 2020) and preliminary data from 1950 to 1958 (Bell et al. 2021). These data are available at 0.25° x 0.25° resolution.

A significant disparity exists among gridded precipitation observations over the AP due to the relatively low density of station observations (Zittis, 2017; Patlakas et al., 2021). Therefore, we use multiple gridded observations and the reanalyzed precipitation from ERA5 to improve robustness. The comparison of reanalyzed and grid-based observed precipitation guides the determination of the parts of AP where results should be considered relatively reliable. As many gridded observations do not include data before 1979, we limit these comparisons to four datasets, including only those observations that extend through most of our analysis period: the University of East Anglia Climate Research Unit (CRU, Harris et al., 2014), the Global Precipitation Climatology Centre (GPCC, Schnieder et al., 2020), the University of Delaware (UDel, Matsuura & Willmott, 2018) and the Climatology Lab's TerraClimate (Abatzoglou et al., 2018) monthly precipitation products. All datasets are re-mapped to ERA5 resolution using bilinear interpolation for comparison. Data from CRU, GPCC, and UDel is only available through 2020, 2019, and 2017 respectively, while TerraClimate is not available before 1958, so only common seasons across datasets are considered in comparisons.

2.2. Modes of Variability

We consider 14 natural modes of climate variability in investigating AP precipitation global teleconnections (Table 1), including ENSO, IOD, PDO, Tropical Western Eastern Indian Ocean Dipole (TWEIO; Abid et al., 2020), Tropical South Atlantic Index (TSAI), SH, NAO, EAM, West Pacific Pattern (W. Pac), East Pacific/North Pacific Pattern (EP/NP), Pacific/North American Pattern (PNA), EAWR, Scandinavia Pattern (SCAND), and Polar/Eurasian Pattern

(POL/EUR). ENSO is represented using three indices: Niño3, Niño4, and Niño3.4 (see Table 1). Index values for the PDO are obtained from the National Center for Environmental Prediction at https://www.ncei.noaa.gov/pub/data/cmb/ersst/v5/index/ersst.v5.pdo.dat. Index values for the NAO, EAM, W. Pac, EP/NP, PNA, EAWR, SCAND, and POL/EUR are obtained from the National Center for Environmental Prediction (NCEP) at https://ftp.cpc.ncep.noaa.gov/wd52dg/data/indices/tele_index.nh. The NCEP calculates indices by implementing a rotated Principal Component Analysis on the first 10 Empirical Orthogonal functions (EOFs) of monthly 500 hPa Geopotential (Barnston and Livezey 1987). These EOF-based indices are orthogonal at a monthly scale, but their seasonal subsets may have non-zero correlations.

We additionally calculate the remaining indices, shown in Table 1, by finding the area-weighted mean anomaly from the climatology (1950 to 2021) of the specified variable over the given area. Each of these indices is standardized before its application. The use of multiple ENSO indices (Niño3, Niño3.4, and Niño4) is to establish a robust understanding of the role of SST variability in the eastern, east-central, and central Pacific. TWEIO is used similarly to Abid et al. (2020), who showed that it could potentially modulate ENSO influence over remote regions. Likewise, SH has also been shown to have positive teleconnections with AP temperatures (Hasanean et al., 2013). TSAI is very similar to Enfield and Mayer (1997), but the area considered in this study is extended from 20°S to 30°S.

Index	Variable	Region/calculation	Source
PDO	SST	Leading EOF 20°N – 90°N, 110°W-110°E	NCEI
NAO EAM W. Pac EP/NP PNA EAWR SCAND POL/EUR	500 hPa GPH	Rotated EOFs (mode associated with each index varies by month) 20°N – 90°N, full hemisphere	NCEP

ENSO	SST	5°S - 5°N, 150°W-90°W – NIÑO3 5°S - 5°N, 170°W-120°W – NIÑO3.4 5°S - 5°N, 160°E-150°W – NIÑO4	Calculated
TWEIO	Precipitation	(10°S - 10°N, 40°E-80°E) – (10°S - 10°N, 90°E-140°E)	
TSAI	SST	30°S - 0°, 30°W-10°E	
IOD	SST	(10°S - 10°N, 50°E-70°E) – (10°S - 0°, 90°E-110°E)	
Sib. High	SLP	40°N - 65°N, 80°E-120°E	

Table 1. Definitions for the 14 modes of variability and three modes of ENSO used through the rest of the paper.

2.3. Analyses

The AP is defined following Horan et al. (2022) as the Asian continent south of the Turkish border and west of the Iranian border. This includes the portions of Iraq and Syria that are not formally considered part of the Peninsula. In this study, a sub-selection of the AP region is made based on the consistency of precipitation distribution across observations (see section 3a). The wet season is split into two parts: one from November through February (winter) and one consisting of March and April (spring) to investigate the persistence (or lack thereof) of global teleconnections.

The EOF analyses are performed to identify the modes of AP precipitation variability. The first three EOFs and their associated Principal Components (PCs) are considered for investigating precipitation variability. Furthermore, the detrended 500 hPa global GPH and SSTs over 30°S – 60°N are regressed onto PCs to determine if the first three precipitation modes of variability can be associated with any of the known naturally occurring oceanic or atmospheric patterns. We complete these analyses for both the winter and the spring for three time periods: 1) the entire length (November 1950 to April 2021), 2) the first half (early; November 1950 to April 1986), and 3) the second half (late; November 1986 to April 2021). This data split is used to gain insight into the potential shifts or other changes in global teleconnections, such as those seen by Kang et al. (2015) for ENSO. Note that where to split the dataset in our analyses (between 1975 and 1990) had little impact on most EOF patterns and associated regressions of SST and GPH.

Next, each index's winter and spring averages are obtained and detrended, then detrended AP precipitation is regressed onto each index for both winter and spring for early and late periods. Finally, the Pearson correlation coefficients are calculated for a 21-year rolling period (beginning with Nov 1950 to April 1971 and ending with Nov 2010 to April 2021) between all 14 indices

and between indices and three PCs in winter and spring. The statistical significance in all analyses is based on a two-tailed Student's t-test with N-2 degrees of freedom at the 90% confidence level.

3 Results

3.1. Precipitation distribution uncertainty in datasets

The arid nature of the AP region, combined with the limited density of surface observations, creates significant uncertainty in the gridded observations and reanalysis over this region. Earlier efforts studying the remote influences on AP precipitation have largely ignored investigating the robustness of findings within the context of data-driven uncertainty in global teleconnections. Here we first identify the AP region where uncertainty in precipitation is significant across the gridded observations or reanalysis and restrict our analyses to those parts of AP where relatively higher confidence exists. This sub-selection of the AP region is achieved by performing a pairwise correlation between the datasets (CRU, TerraClimate, GPCC, UDel, ERA5) over the period shared in each case (Fig. 1, Supplementary Fig. S1). The correlation remains relatively high (>0.5) between ERA5 and all datasets to the north of Saudi Arabia and in the eastern half of Saudi Arabia, with some small areas of exception in central Iraq. ERA5 correlates best with TerraClimate because it blends station-based gridded observations and reanalysis (Abatzoglou et al. 2018). The correlation between all datasets is consistently weak along the Red Sea coast, Yemen, and Western Oman (<0.5) (Fig. 1, Supplementary Fig. S1). There is more consistency between ERA5 and GPCC in northwest Saudi Arabia in a more recent period (not shown), however, inconsistencies persist through Yemen and southwest Saudi Arabia. Note that attributing precipitation variability in gridded observations to global teleconnections depends on using dynamic and thermodynamic surface and atmospheric state variables from the reanalysis. Therefore, regions with poor consistency between reanalyzed and observed precipitation risk identifying inaccurate large-scale drivers for precipitation variability. Therefore, this study on global teleconnections of AP precipitation is restricted to those parts of AP that exhibit relatively

high consistency between observations and reanalysis. The sub-selected AP region includes areas north of 22°N – a line from the Egypt–Sudan border to the eastern corner of Oman.

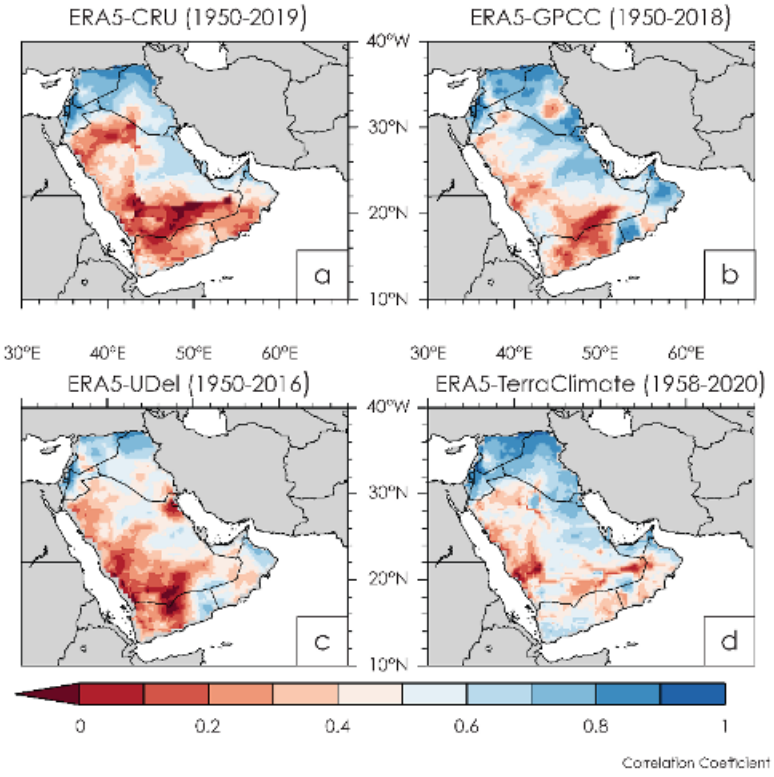

Figure. 1. Correlation Coefficients (unitless) between ERA5 and a) CRU, b) GPCC, c) UDel and d) TerraClimate over the specified timeframe.

3.2. Modes of AP precipitation variability

While the general climatology of this reason has been discussed in previous research, (Almazroui et al., 2012; Almazroui, 2011; Edgell, 2006; Abdullah and Al-Mazroui, 1998; Almazroui et al., 2013), and simple overview of the mean, standard deviation and trends of wet season, winter, and spring variability is available to the reader in Supplementary Figure S2. Of note, particularly with regards to trends, this climatology extends longer than previous research and many of the previous wet season drying trends (Almazroui & Saeed, 2020; Donat et al., 2014, Syed et al., 2022, Horan et al., 2022) are not as apparent as an analysis that focuses only on the most recent 40 years. The structure of variability in winter precipitation over AP is described using the first three EOFs that collectively explain more than 67% of the variance for the entire 71-year period (Fig 2, PC Time Series in Fig. S3), and 63% and 75.2% variance for early (1950–1986, Fig S4 and late (1986–2021, Fig S5) periods, respectively. The first EOF (EOF1) spatial pattern in winter consistently displays high precipitation in the northern part of the domain, steadily decreasing in central Saudi Arabia in all cases (entire, early, and late periods). For the entire length, the EOF1 accounts for 42.1% of the variance but shows an increase from 36.4% to 48.1% when analyzed separately for early and late periods. The second EOF (EOF2) shows a dipole between a dryer pattern at the Turkish border, where the AP region receives maximum precipitation during winter (Horan et al., 2022), and a wetter pattern in southern Iraq and central

Saudi Arabia. The spatial distribution of the EOF2 pattern shows a close resemblance between the entire length and the early period though the wetter region during the early period is concentrated over central Saudi Arabia (Figs. 2, S3). Like EOF1, the explained variance increases from 16.9% in the early period to 19.7% in the late period (Figs. S4-S5). The third EOF (EOF3) consistently shows a dry-wet-dry pattern with a noticeably wetter pattern spanning over northern Saudi Arabia/southern Iraq and a dryer pattern over east-central Saudi Arabia, United Arab Emirates (UAE), and eastern Oman. A dry anomaly is also present over parts of Syria.

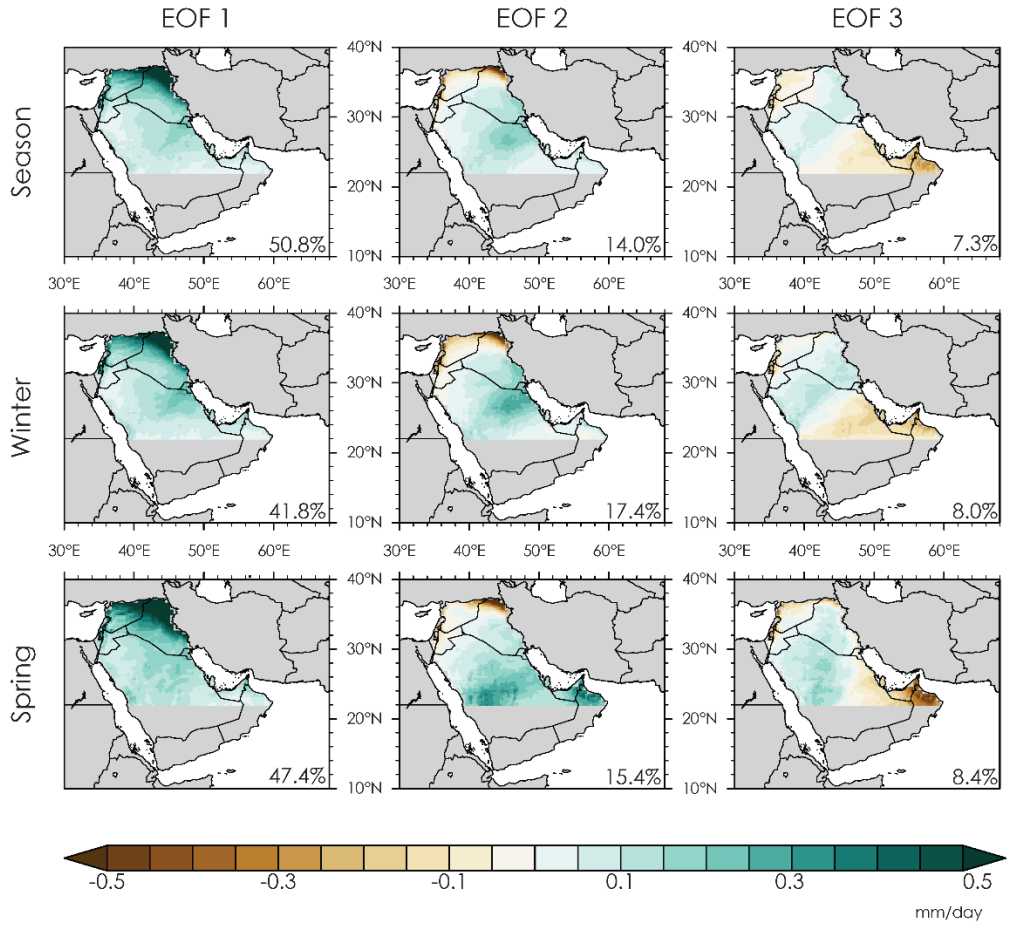

Figure 2. The first three EOFs (in mm/day) during (first row) the full wet season from November to April, (second row) winter months from November through February and (third row) spring months consisting of March and April. The amount of variability explained by each EOF during their respective season is indicated in the bottom right corner of each map.

Like the EOF analyses for winter precipitation, the structure of variability in spring precipitation is described using the first three EOFs that collectively explain more than 71.2% of the variance for the entire 71-year period (Fig. 2), and 77.1% and 68.4% variance for the early and late periods, respectively (Figs. S4-S5). Contrary to the winter, where the first three EOFs explain more variance in the late period of the analyses, the collectively explained variance of spring precipitation through the first three EOFs decreases in the late period. Spatially, the three

EOFs for the spring precipitation show patterns like the ones seen in the corresponding winter EOFs when the entire 71-year period is considered. However, compared to the winter, we note that the above or below-average conditions depicted in all EOFs are substantially more robust in the spring (Fig 2). As stated earlier, the explained variance using the first three EOFs decreases during the late period (Figs S4-S5). Most of this reduction comes from EOF1, which decreases from 52% in the early period to 43.7% in the late period. As a result, the spatial pattern of above-average precipitation in EOF1 is relatively subdued over Saudi Arabia in the late period. Interestingly, the spatial variation in EOF1 over Saudi Arabia during the early and late periods is opposite to what we notice during the winter (Figs. S4-S5).

3.3. Modes of AP precipitation variability and global teleconnections

To gain insight into the potential influence of naturally occurring modes of climate variability on AP precipitation, we regress the 500 hPa GPH and global SST anomalies on the first three leading PCs of AP precipitation (Figs 3-6). The regression with SSTs should highlight areas in oceanic basins with a potential role in inducing these patterns of precipitation variability over the AP region. On the other hand, regression with GPH should reveal dynamic patterns associated with each of the three modes of AP precipitation variability, some of which may be recognizable as the commonly occurring internal modes of atmospheric variability in the Northern Hemisphere. The regressions are performed separately for winter and spring.

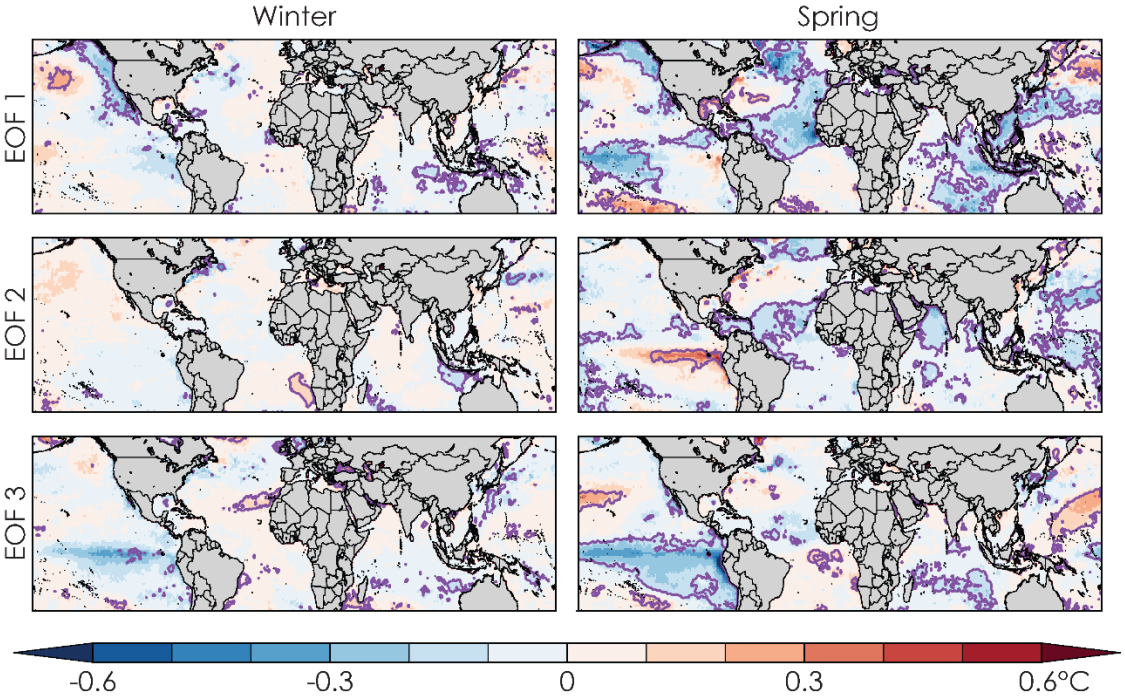

Figure 3. The (left, winter) November through February and (right, spring) March and April regression of the (top row) first, (middle row) second, and (bottom row) third Principal components of AP Precipitation onto 30°S-60°N SST (°C per 1 standard deviation in PC) between the 1950-1951and 1985-1986 wet seasons. Areas outlined in purple indicate areas where correlations are statistically significant ($p < .10$).

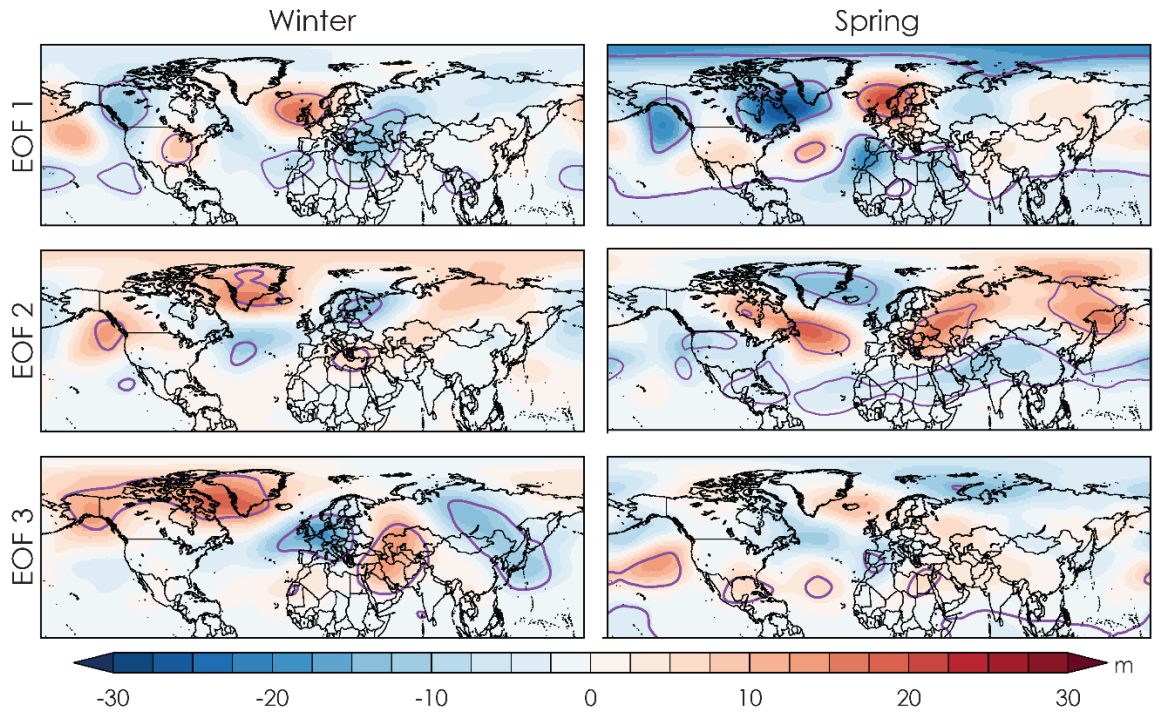

Figure. 4. Same as Figure 3 except for GPH (m per 1 standard deviation in PC)

In the winter of the earlier period (1950–1986), the regressions of global SST anomalies (Fig 3) reveal a lack of linkages with any of the oceanic basins except in the case of the first PC (PC1), which displays a pattern of significant association with the Pacific Ocean SSTs, north of 20°N, resembling negative PDO. The regressions of global SST anomalies in spring exhibit patterns strikingly different from those in winter. All three modes display a significant negative association with the tropical SSTs, including equatorial central Pacific (Niño4 region), equatorial Atlantic, and the eastern Indian Ocean in the case of PC1, tropical Atlantic, western Pacific, and Indian Oceans in the case of second PC (PC2), and equatorial Pacific in the case of third PC (PC3). Moreover, in PC2 regression, a significant positive association exists in the eastern tropical Pacific (Niño3 region).

In the winter of the earlier period, the regressions of three PCs onto GPH anomalies (Fig. 4) exhibit distinct patterns. The PC1 regression displays a significant negative GPH anomaly over AP, representing the strengthening of the subtropical westerly jet over the region and supporting wetter-than-normal conditions. The anomaly over the Pacific, north of the equator, represents a negative PDO pattern consistent with the corresponding SSTs regression. The PC2 regression displays a weak and insignificant dipolar GPH anomaly pattern with the positive in the northern portions of the AP and negative over Scandinavia, consistent with the distribution of dry precipitation anomaly over Northern Iraq and Syria in EOF2 of AP precipitation (Fig. 2). The characteristics of a negative NAO phase are also present over the northern Atlantic. The PC3 regression reveals a negative EAWR pattern (Barnston & Livezey, 1987) over the Eurasian

region, with positive GPH anomalies extending over the central AP region, partly consistent with the below-normal precipitation pattern in EOF3 over parts of AP (Fig 2, S4).

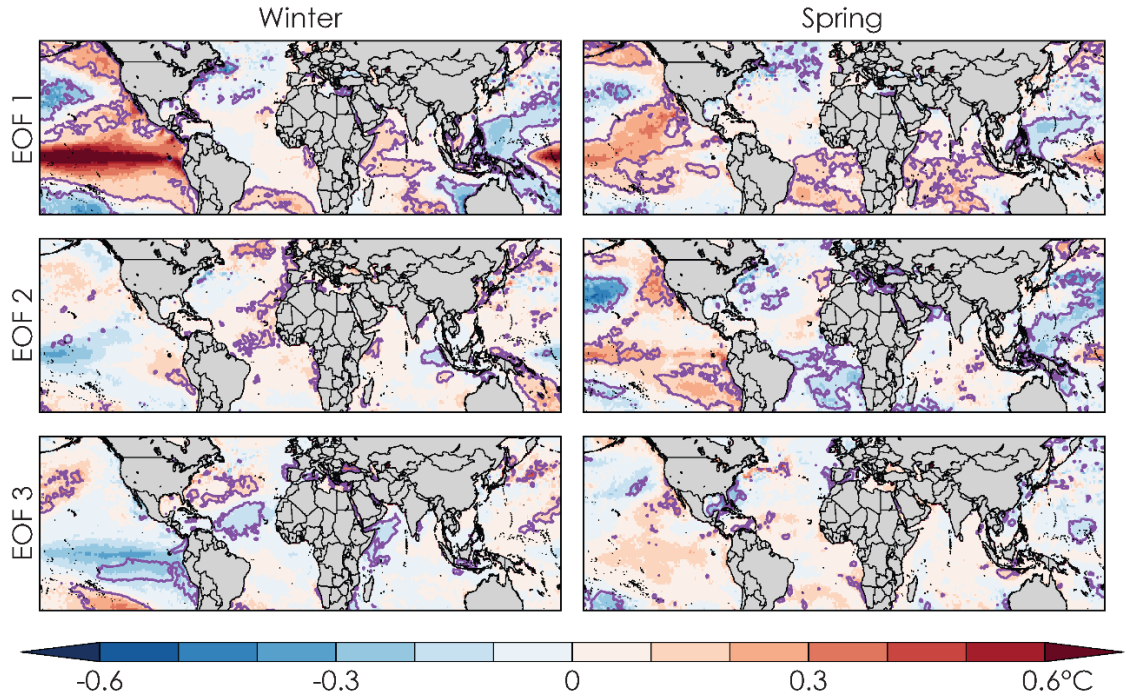

Figure 5. Same as Figure 3 except for the wet season from 1986-1987 through the wet season from 2020-2021.

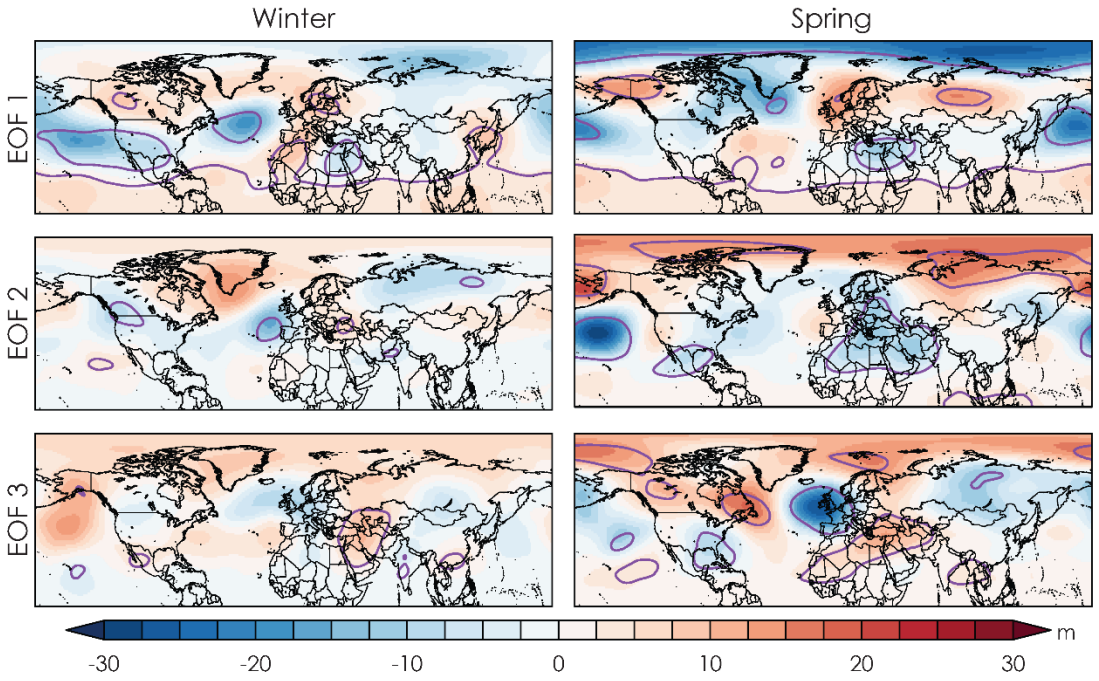

Figure 6. Same as Figure 3 except for GPH for the wet season from 1986-1987 through the wet season from 2020-2021.

The GPH anomalies associated with spring PCs exhibit some commonalities with corresponding patterns seen in winter (Fig. 4). The strengthening of the subtropical westerly jet over AP in PC1 regression, the dipole pattern in PC2 regression, and the weakening of the subtropical westerly jet in PC3 regression are similar in the two seasons. However, the dipole pattern in the PC2 regression is significant and robust in spring (Fig 4), which is consistent with the stronger precipitation anomalies pattern seen in spring EOF2 (Fig 2). Similarly, the weakening of the subtropical jet is no longer significant in PC3 regressions. Beyond the AP region, no recognizable atmospheric mode of Northern Hemisphere variability emerges except in the PC2 regression, where the GPH anomaly pattern resembles the positive NAO phase.

A dramatic shift in the potential role of oceanic modes is witnessed in winter during the late period (Figs. 5-6). For instance, SST regression onto PC1 reveals a robust positive association with the equatorial pacific over the ENSO region and the western Indian Ocean. Likewise, PC3 regression onto SSTs shows a relatively less strong but significant negative association with Atlantic and Pacific Niño regions. Interestingly, on the other hand, when compared to the early period (Fig. 3), the role of oceanic modes also displays shifts or lack of robustness in spring. For instance, PC3 does not significantly relate to SSTs in the tropical oceans. The positive association with the ENSO region in PC2 regression is spatially more robust, while the negative association in the Atlantic region now shifts to the tropical south Atlantic extending as far south as 30° south. Moreover, PC1 regression shows a positive association with SSTs in the tropical oceans, which is opposite to the spring of the earlier half. (Figs 3, 5)

3.4. AP precipitation regression onto indices

The PC regressions onto global SSTs and GPH anomalies unravel those broad areas in global oceans and atmosphere that may have a physical linkage with precipitation variability over the AP region. The emerging patterns over some of these areas represent recognizable natural modes. Therefore, to further identify specific roles that natural modes of climate variability may have in precipitation distribution over the AP region, we regress AP precipitation onto 16 indices

representing 14 natural modes of climate variability (See Table 1). The regressions are performed separately for winter, spring, and the two periods (Figs.7-8, S6-S9).

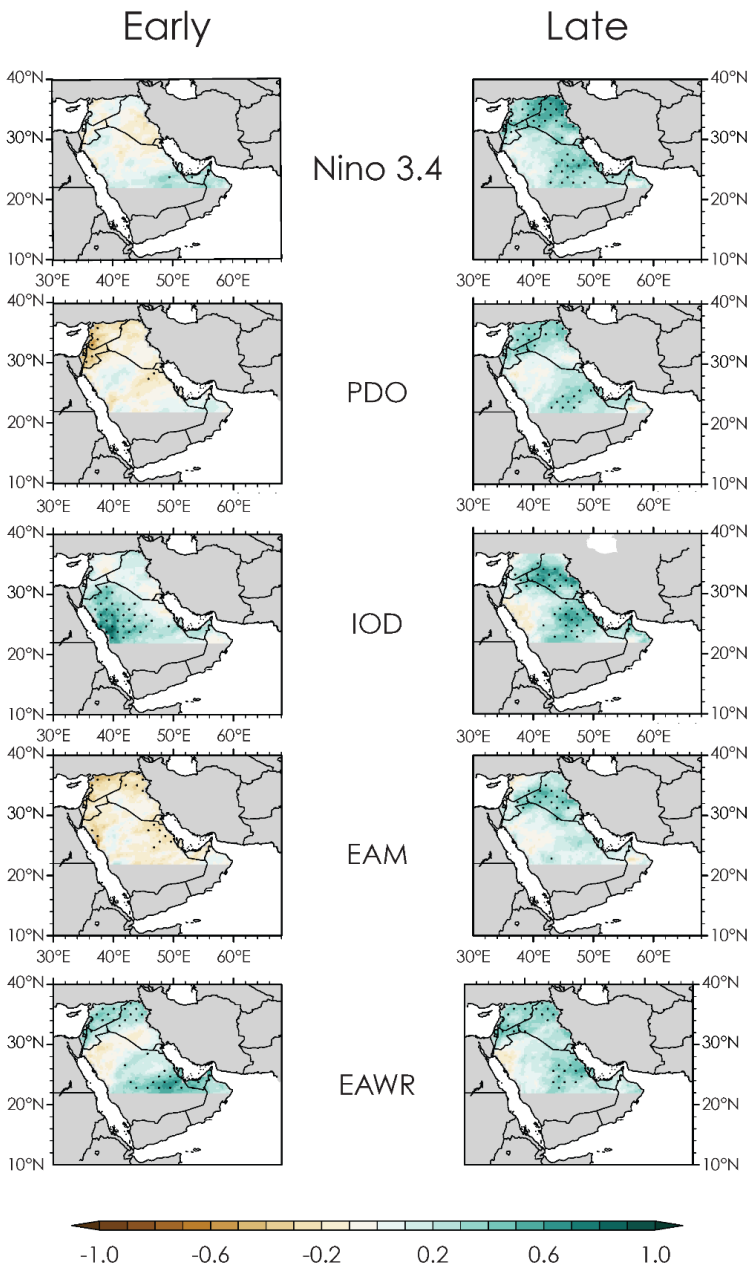

Figure 7. The regression of AP Precipitation on key climate indices (standard deviation of local precipitation per standard deviation of the index) from (left) the winter (Nov – Feb) of 1950-1951 through the winter of 1985-1986. and (right) the winter of 1986-1987 through the winter of 2021. Stippling indicates areas where the correlation between the index and precipitation is statistically significant (p<.10). All indices are shown in Figures S5 and S6.

353

354 Several modes display spatiotemporally varying influence on AP winter precipitation. ENSO (all
355 indices, Figs 7, S6) show little to no effect on precipitation variability in the winter of the early
356 period, which dramatically changes to a widespread significant positive influence in the later
357 period (Fig 7, S7). The PDO exhibits limited negative impact over the northern parts of the
358 Peninsula in the early period, reversing to a spatially more substantial positive influence over the
359 central and north AP regions later. The same is true in the case of EAM, POL/EUR, and EP/NP.
360 IOD influence is significantly positive over the western parts of AP, which spatially switches to
361 the eastern regions in the late period. The only exception is EAWR, which consistently displays
362 a similar pattern of significant positive influence in both periods. This may be due to increased
363 (decreased) evaporation from the Red Sea during the positive (negative) phase of EAWR
364 (Abualnaja et al., 2015).

365

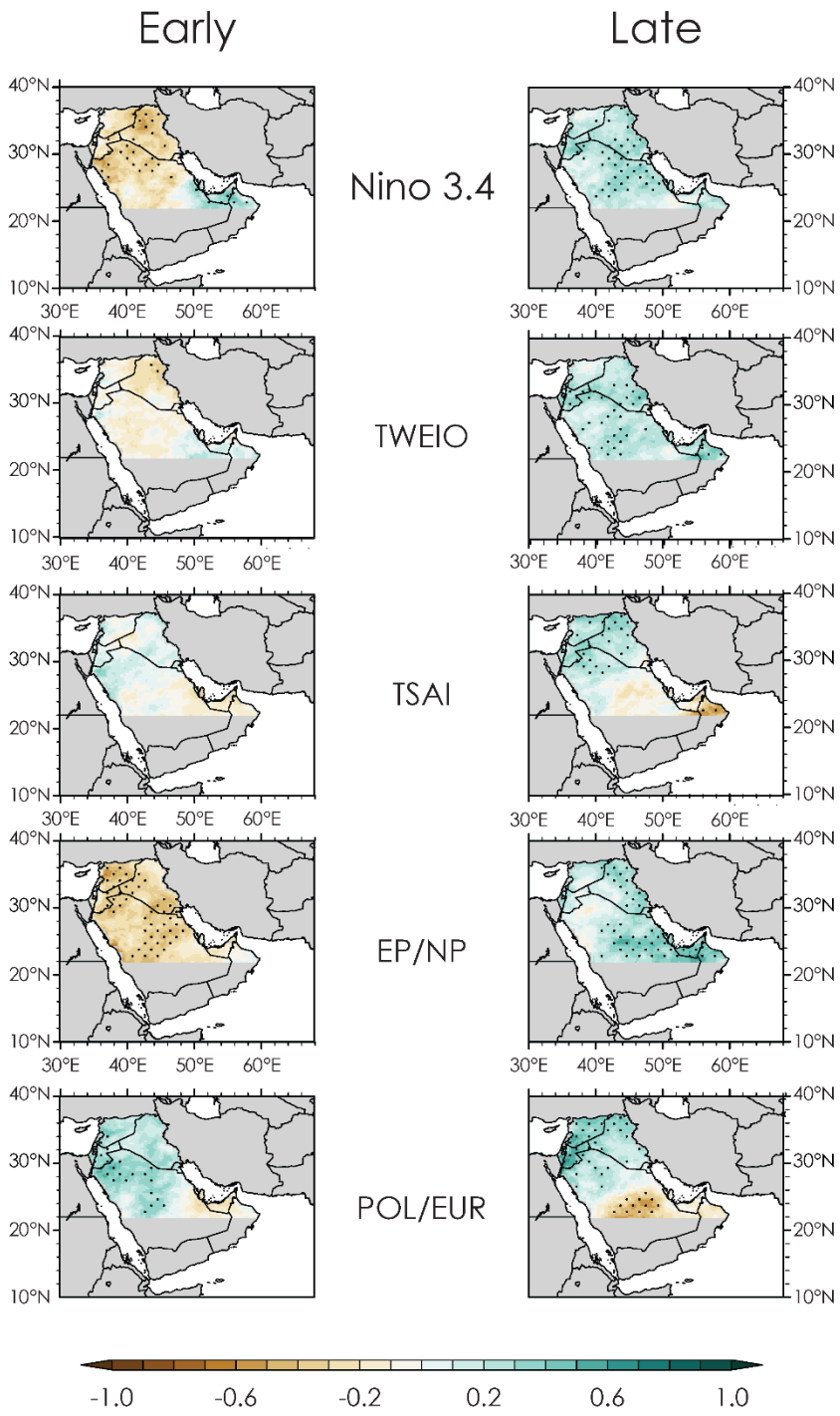

366

367 **Figure 8**. The regression of AP Precipitation on key climate indices (standard deviation of local precipitation
368 per standard deviation of the index) from (left) the spring (Mar – Apr) of 1951 through the spring of 1986. and
369 (right) the spring of 1987 through the spring of 2021. Stippling indicates areas where the correlation between
370 the index and precipitation is statistically significant ($p<.10$). All indices are shown in Figures S7 and S8

The spatiotemporal variability of global teleconnections of AP precipitation persists in spring (Figs 8, S8-S9). However, the characteristics of these variations are distinct between winter and spring. In the early period, central and western Pacific-based ENSO indices (Niño3.4, Niño4, Fig S8) display a strong negative association except over parts of Oman and UAE, while the Indian Ocean-based TWEIO and eastern Pacific-based Niño3 index exhibit no Influence. Contrarily, all ENSO indices and TWEIO show significant positive associations throughout the AP region in the late period (Figs 8, S9). EAM, W. Pac, and EP/NP display a robust negative association in the early period, which shifts to insignificant influence in the case of EAM and W. Pac (Figs. S8-S9), and a significant positive impact in the case of EP/NP during the late period (Fig. 8). The IOD influence also shifts from widespread significant positive to considerably limited negative regressions (Figs. S8-S9). TSAI and PNA show substantial positive impacts in the late period but no influence in the early period. The only exception is POL/EUR, which consistently delivers a significant positive influence in the northern AP in both periods and a somewhat negative effect in the lower parts (Fig. 8). However, the negative impact is only robust in the late period.

4 Discussion

Several key points can be derived from our analysis of AP precipitation variability and its global teleconnections. While precipitation generally shows similar patterns of variability when aggregated at the wet season, winter, and spring levels, some crucial distinctions can still be drawn. The robustness of EOF patterns varies between winter and spring (Fig. 2), and so does the temporal variation in the associated explained variances. More importantly, the role of naturally occurring oceanic and atmospheric variability in projecting winter and spring EOF patterns, which are visibly similar, onto the AP displays sharp disparities. For instance, the ENSO role only becomes visible in the late period in winter, while it shows influence in both periods in spring (Figs. 3,5,7-8). Moreover, EAWR displays a strong impact in winter but little to no influence in spring (Figs 7, S8-S9). Spatiotemporal heterogeneities in the role of several other modes also exist. Additionally, stronger subtropical jet and lower GPH anomalies through northern Africa are more associated with spring variability than winter (Figs 4,6). While much of the previous research investigating AP precipitation has considered the entire wet season (Abdullah & Al-Mazroui, 1998; Abid et al., 2020; Almazroui, 2011; Atif et al., 2020; Horan et al., 2022; Kang et al., 2015) , and some others have focused on only the winter months (Abid et al., 2016; Saeed & Almazroui, 2019), these distinctive comparisons between winter and spring suggest that separating the wet season into two separate parts is necessary to accurately determine the large-scale processes shaping precipitation variability over the region.

The spatial variability in SST anomalies in the equatorial Pacific (ENSO flavors) also plays a role in AP precipitation variability. For instance, in the early period spring, Niño3 exhibits a limited positive association over parts of eastern AP, while Niño4 has a widespread negative influence (Fig S8). Likewise, Niño3's positive impact over central AP is more robust than Niño4 in winter (Figs S6-S7). Therefore, ENSO diversity should be a consideration while investigating AP precipitation variability. The results also clearly manifest the varying influence of several natural modes of variability over time. ENSO transitioned from little impact to a significant positive effect in the winter (Figs S4-S5). The Niño3.4 and Niño4 correlate negatively with AP

precipitation in the early period spring but are positively associated with the central and western equatorial Pacific in the late period spring (Figs S8-S9).

Similarly, while the IOD maintains a positive correlation with AP precipitation in winter of both periods, in spring, its influence reverses from positive to negative over Kuwait and central Saudi Arabia over time (Figs S8-S9). Moreover, the most consistent teleconnection from the Northern Hemispheric atmospheric modes of variability in the winter comes through the EAWR pattern, which positively impacts winter precipitation in both periods (Fig. 7). However, EAWR shows little influence on spring precipitation (Figs S8-S9). Conversely, while the POL/EUR pattern shows a clear dipole between northern and southern regions during the late period and a dipole between northwest and southeast in spring of the early period in the spring (Fig. 8), during the winter, POL/EUR does not show a significant correlation with AP precipitation in most areas, transitioning from an insignificant dry correlation to an insignificant wet correlation (Figs. S6-S7). Finally, while the tropical south Atlantic Ocean shows little impact on winter and early spring periods (Figs S6-S8), it displays significant dipolar influence between precipitation in the northern portion of the AP and that near the Gulf of Oman during the late period spring (Fig. S9).

Note that analyses thus far have focused on each index individually. However, a significant interaction between oceanic and atmospheric modes while propagating their remote influences is typical. Mehmood et al. (2022) note a substantial role of interactions within extratropics and between tropics and extratropics in global teleconnections of precipitation variability over central and southwestern Asia in the cold season. Atmospheric diabatic heating anomalies induced by tropical forcing often propagate eastward Rossby waves in the higher latitudes. In the Northern Hemisphere, these Rossby waves can interact with each other when multiple tropical forcing coexists and with the internal modes of atmospheric variability. Thus, understanding global teleconnections of AP precipitation would remain incomplete without considering interactions

between natural modes of variability. We investigate these interactions using the 21-year moving correlations between all indices spanning the entire analysis period (Figs 9-10, S10-S11).

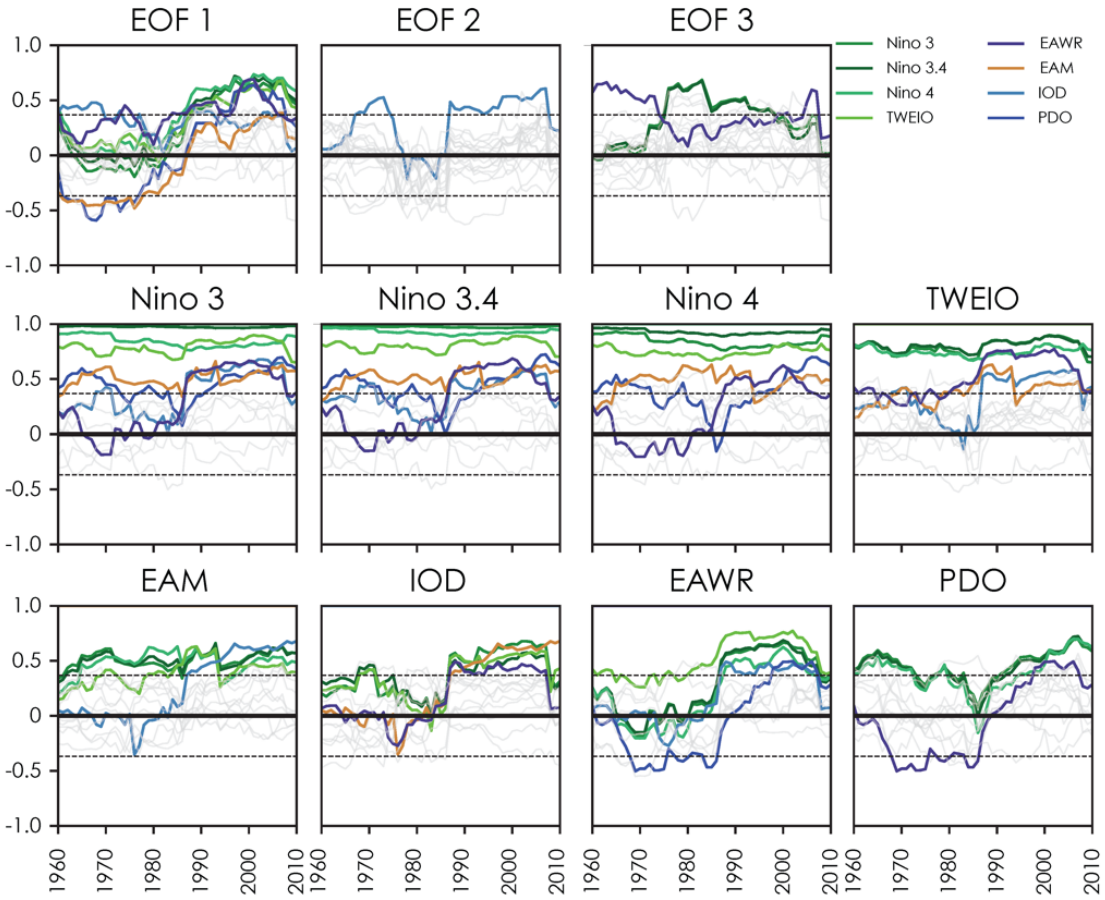

Figure 9. Rolling 21-year correlations during the winter months (Nov – Feb) for all indices that reach statistical significance with at least one EOF for 17/51 wet seasons with all other indices and all 3 EOFs. Years on the horizontal axis indicate the mid-point of the 21-year correlation. Dotted lines indicate statistical significance in correlations ($p<.10$). All indices are shown in Fig. S10.

During winter (Figs. 9, S10, early/late period full correlation values shown in Table S1-S2), the first EOF manifests interactions within the extratropics and between the tropics and extratropics. In the early period, PDO and EAM are the two natural forcings that significantly correlate negatively with the EOF1. Interestingly, during this period, EAM exhibits high correlations with indices representing ENSO, TWEIO, and W. Pac, which have high correlations among them (Fig. 9). These interactions suggest that while tropical forcings, such as ENSO, do not directly impact the AP precipitation variability described in EOF1 of the early period, they may indirectly influence via their projections onto EAM. The same is partly true in the case of PDO, which exhibits varying but most significant relationships with ENSO indices during the winter of the early period. The relationship of PDO and EAM with EOF1 becomes insignificant in the 80s and reverses to positive in the late period, but only PDO's influence becomes significantly

positive. The late period is also the time when all ENSO indices and TWEIO display significant correlations with EOF1. EAWR relationship with EOF1 remains consistently positive, shows multi-decadal variability in the early period, and then becomes relatively strong and stable in the late period, which coincides with the time when EAWR exhibits strong correlations with ENSO indices and TWEIO. Note that EAWR also exhibits a significant negative relationship with several extratropical modes of variability (particularly SH), which have no direct role in shaping the first mode of AP precipitation variability (Fig S10). Therefore, these interactive relationships suggest that ENSO and TWEIO have both direct and indirect influences (via EAWR) on AP precipitation variability manifested in EOF1. Similarly, extratropical forcings, such as SH, may also indirectly impact the AP precipitation distribution via EAWR.

The IOD is the only natural mode with a meaningful relationship with the winter EOF2 other than in the 1980s when this relationship disappears (Fig. 9). The temporal variability in the IOD relationship coincides nicely with the variation in IOD correlation with ENSO indices, TWEIO and TSAI, which suggests an indirect role of these forcings. The same is true in the case of EAM, which displays a strong correlation with IOD in the late period. EOF3 shows the role of SST variability in the central and western Pacific and EAWR. Interestingly, EAWR's

relationship with EOF3 is strong when the west and central Pacific SST's relationship is weak and vice versa.

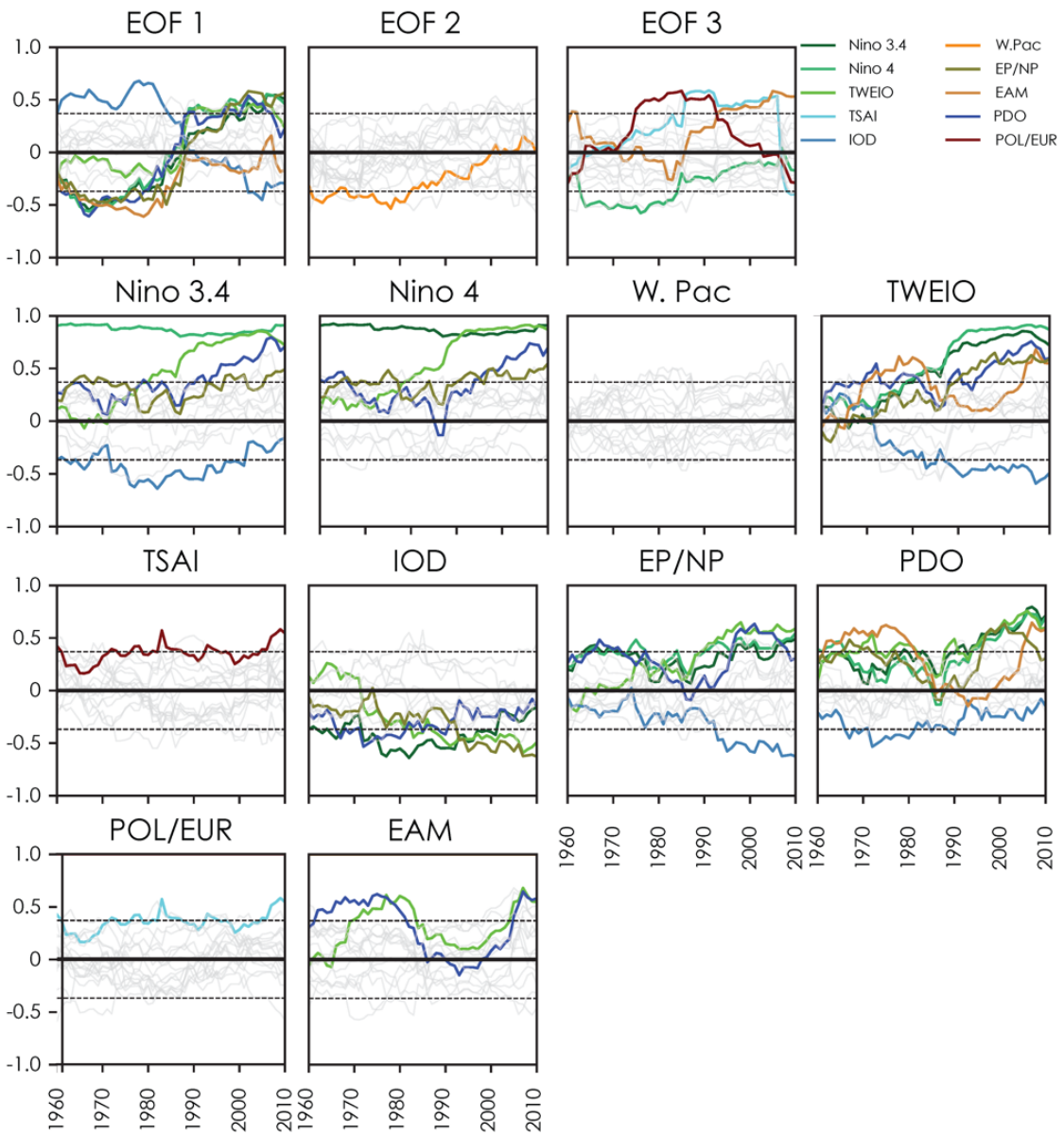

Figure 10. Same as Figure 9 but for spring months (Mar–Apr). All indices are shown in Figure S11.

During the spring (Figs. 10, S11, early/late period full correlations in Tables S3-S4), EOF1 shows a positive IOD and negative influences of central and western equatorial Pacific SSTs (Niño3.4, Niño4), PDO, EP/NP, and EAM. PDO and EP/NP correlate positively with Niño3.4 and Niño4 during this period, while EAM correlates positively with PDO. As previously noted, the IOD influence reverses after the 1980s and remains mostly weak and negative during the rest of the late period. At the same time, all negatively influencing forcings change to positive except for EAM, which becomes irrelevant. The TWEIO influence also reverses from weak negative in the early period to significant positive in the late period. EOF2 only correlates significantly to the

W. Pac, which has no noticeable relationship to any other forcing throughout the analysis period. EOF3 in spring shows a strong negative influence of western equatorial Pacific SSTs (Niño4) in the early half, a strong positive effect of POL/EUR through the 1980s, and a strong positive influence of TSAI in the late period. Note that POL/EUR exhibits a high correlation with TSAI throughout the analysis period, suggesting that TSAI may have both direct and indirect relationships with the third EOF (Fig. 10). Overall, these analyses suggest substantial variability in the roles of several naturally occurring climate modes in shaping the AP precipitation variability. Additionally, tropical-extratropical interactions exhibit an important role in establishing teleconnections of natural modes in tropical oceans.

5 Conclusions

We thoroughly examine precipitation variability over the AP regions, its linkage with naturally occurring oceanic and atmospheric modes, and spatiotemporal variations in those teleconnections. The first three EOFs of AP precipitation, which explain ~70% of the variance, suggest intra-seasonal and multi-decadal variations in the characteristic of precipitation variability. These EOFs are consistent amongst the seasons and allow future work to recognize the patterns seen in precipitation over the region. Linear regression analysis unravels a complex network of global teleconnections where often more than one natural modes of climate variability are at play. The influence of several of these modes displays a shift in the 1980s. The key findings based on these analyses are as follows:

1) Consistent with previous research (Zittis, 2017), our analysis reveals inconsistency in precipitation observations in the southern portion of the AP and emphasizes the consideration of data-based uncertainty.

2) The patterns of precipitation variability and their global teleconnections display substantially different characteristics in the winter and spring seasons. Therefore, using November –April as a wet season for investigating drivers of precipitation variability and change may be misleading.

3) ENSO plays a key role in precipitation variability over the AP. However, ENSO diversity plays a role in shaping its influence over the AP region. Moreover, while the direct ENSO influence only becomes more robust after the 80s, as noted in Kang et al. (2015), the indirect ENSO influence through its projection onto Northern Hemisphere atmospheric modes, such as EAM and EAWR, or through inter-basin interaction (e.g., via the Indian Ocean) persists throughout the analyses period.

4) The Northern hemisphere modes of atmospheric variability are important in establishing interactions within the extratropics and tropics-extratropics. These interactions partly meditate tropical (ENSO, TSAI, TWEIO) and extra-tropical (SH, PDO) teleconnections over the AP region.

5) Several teleconnections of AP precipitation exhibit a shift in the 1980s. While some of these changes may be related to using satellite data in reanalysis, further investigations are warranted to understand the causes of these shifts fully. Moreover, with growing uncertainty over the future of ENSO (Lee et al. 2022) other teleconnections

522 may dominate future precipitation variability and may be exhibiting a further shift. Future
523 targeted modeling analysis may provide insight into the dynamical origins of these
524 precipitation patterns.

525 **Acknowledgments**

526 This work is the supported by the U.S. Air Force Numerical Weather Modeling Program and
527 National Climate-Computing Research Center, which is located within the National Center for
528 Computational Sciences at the ORNL and supported under a Strategic Partnership Project, 2316-
529 T849-08, between DOE and NOAA. This research used resources of the Oak Ridge Leadership
530 Computing Facility, which is a DOE Office of Science User Facility supported under Contract
531 DE-AC05-00OR22725.

532 **Open Research**

533 ERA5 data are available online
534 (https://www.ecmwf.int/en/forecasts/datasets/reanalysis/datasets/era5)
535 CRU Data are available online
536 (https://catalogue.ceda.ac.uk/uuid/edf8febfdaad48abb2cbaf7d7e846a86)
537 GPCC Data are available online (https://psl.noaa.gov/data/gridded/data.gpcc.html)
538 TerraClimate Data are available online (https://www.climatologylab.org/terraclimate.html)
539 UDel Data are available online
540 (http://climate.geog.udel.edu/~climate/html_pages/Global2017/index.html)
541

542 **References**

543 Abatzoglou, J. T., Dobrowski, S. Z., Parks, S. A., & Hegewisch, K. C. (2018). TerraClimate, a
544 high-resolution global dataset of monthly climate and climatic water balance from 1958-2015.
545 Scientific Data, 5(1), 1–12. https://doi.org/10.1038/sdata.2017.191

546

547 Abdullah, M., & Al-Mazroui, M. (1998). Climatological study of the southwestern region of
548 Saudi Arabia. I. Rainfall analysis on JSTOR. Climate Research, 9, 213–223. Retrieved from
549 https://www.jstor.org/stable/24864531

550

551 Abid, M. A., Kucharski, F., Almazroui, M., & Kang, I.-S. (2016). Interannual rainfall variability
552 and ECMWF-Sys4-based predictability over the Arabian Peninsula winter monsoon region.
553 Quarterly Journal of the Royal Meteorological Society, 142(694), 233–242.
554 https://doi.org/10.1002/qj.2648
555
556 Abid, M. A., Ashfaq, M., Kucharski, F., Evans, K. J., & Almazroui, M. (2020). Tropical Indian
557 Ocean Mediates ENSO Influence Over Central Southwest Asia During the Wet Season.
558 Geophysical Research Letters, 47(18), e2020GL089308. https://doi.org/10.1029/2020GL089308
559 Abualnaja, Y., Papadopoulos, V. P., Josey, S. A., Hoteit, I., Kontoyiannis, H., & Raitsos, D. E.
560 (2015). Impacts of climate modes on air-sea heat exchange in the Red Sea. Journal of Climate,
561 28(7), 2665–2681. https://doi.org/10.1175/JCLI-D-14-00379.1
562
563 Almazroui, M. (2011). Calibration of TRMM rainfall climatology over Saudi Arabia during
564 1998-2009. Atmospheric Research, 99(3–4), 400–414.
565 https://doi.org/10.1016/j.atmosres.2010.11.006
566
567 Almazroui, M., & Saeed, S. (2020). Contribution of extreme daily precipitation to total rainfall
568 over the Arabian Peninsula. Atmospheric Research, 231, 104672.
569 https://doi.org/10.1016/j.atmosres.2019.104672
570
571 Almazroui, M., Nazrul Islam, M., Athar, H., Jones, P. D., & Rahman, M. A. (2012). Recent
572 climate change in the Arabian Peninsula: annual rainfall and temperature analysis of Saudi

573 Arabia for 1978–2009. International Journal of Climatology, 32(6), 953–966.
574 https://doi.org/10.1002/joc.3446
575
576 Almazroui, M., Abid, M. A., Athar, H., Islam, M. N., & Ehsan, M. A. (2013). Interannual
577 variability of rainfall over the Arabian Peninsula using the IPCC AR4 Global Climate Models.
578 International Journal of Climatology, 33(10), 2328–2340. https://doi.org/10.1002/joc.3600
579 Alsaaran, N. A., & Alghamdi, A. S. (2022). Precipitation climatology and spatiotemporal trends
580 over the Arabian Peninsula. Theoretical and Applied Climatology, 147(3–4), 1133–1149.
581 https://doi.org/10.1007/s00704-021-03878-5
582
583 Atif, R. M., Almazroui, M., Saeed, S., Abid, M. A., Islam, M. N., & Ismail, M. (2020). Extreme
584 precipitation events over Saudi Arabia during the wet season and their associated
585 teleconnections. Atmospheric Research, 231, 104655.
586 https://doi.org/10.1016/j.atmosres.2019.104655
587
588 Barnston, A. G., & Livezey, R. E. (1987). Classification, seasonality and persistence of low-
589 frequency atmospheric circulation patterns. Monthly Weather Review, 115(6), 1083–1126.
590 https://doi.org/10.1175/1520-0493(1987)115<1083:CSAPOL>2.0.CO;2
591
592 Bell, B., Hersbach, H., Simmons, A., Berrisford, P., Dahlgren, P., Horányi, A., et al. (2021). The
593 ERA5 global reanalysis: Preliminary extension to 1950. Quarterly Journal of the Royal
594 Meteorological Society, 147(741), 4186–4227. https://doi.org/10.1002/qj.4174
595

596 Chakraborty, A., Behera, S. K., Mujumdar, M., Ohba, R., & Yamagata, T. (2006). Diagnosis of
597 tropospheric moisture over Saudi Arabia and influences of IOD and ENSO. Monthly Weather
598 Review, 134(2), 598–617. https://doi.org/10.1175/MWR3085.1
599
600 Donat, M. G., Peterson, T. C., Brunet, M., King, A. D., Almazroui, M., Kolli, R. K., et al.
601 (2014). Changes in extreme temperature and precipitation in the Arab region: long-term trends
602 and variability related to ENSO and NAO. International Journal of Climatology, 34(3), 581–592.
603 https://doi.org/10.1002/joc.3707
604
605 Edgell, H. S. (2006). Arabian deserts: Nature, origin, and evolution. Arabian Deserts: Nature,
606 Origin, and Evolution. Springer Netherlands. https://doi.org/10.1007/1-4020-3970-0
607 Ehsan, M. A., Tippett, M. K., Almazroui, M., Ismail, M., Yousef, A., Kucharski, F., et al. (2017).
608 Skill and predictability in multimodel ensemble forecasts for Northern Hemisphere regions with
609 dominant winter precipitation. Climate Dynamics, 48(9–10), 3309–3324.
610 https://doi.org/10.1007/s00382-016-3267-4
611
612 Enfield, D. B., & Mayer, D. A. (1997). Tropical atlantic sea surface temperature variability and
613 its relation to El Niño-Southern Oscillation. Journal of Geophysical Research: Oceans, 102(1),
614 929–945. https://doi.org/10.1029/96jc03296
615
616 Harris, I., Jones, P. D., Osborn, T. J., & Lister, D. H. (2014). Updated high-resolution grids of
617 monthly climatic observations - the CRU TS3.10 Dataset. International Journal of Climatology,
618 34(3), 623–642. https://doi.org/10.1002/joc.3711

Hasanean, H. M., Almazroui, M., Jones, P. D., & Alamoudi, A. A. (2013). Siberian high variability and its teleconnections with tropical circulations and surface air temperature over Saudi Arabia. Climate Dynamics, 41(7–8), 2003–2018. https://doi.org/10.1007/s00382-012-1657-9

Hersbach, H., Bell, B., Berrisford, P., Hirahara, S., Horányi, A., Muñoz-Sabater, J., et al. (2020). The ERA5 global reanalysis. Quarterly Journal of the Royal Meteorological Society, 146(730), 1999–2049. https://doi.org/10.1002/qj.3803

Horan, M., Batibeniz, F., Kucharski, F., Almazroui, M., Abid, M. A., Fu, J. S., & Ashfaq, M. (2022). Moisture Sources for Precipitation Variability over the Arabian Peninsula. https://doi.org/10.21203/RS.3.RS-1136144/V2

Kang, I. S., Rashid, I. U., Kucharski, F., Almazroui, M., & Alkhalaf, A. K. (2015). Multidecadal changes in the relationship between ENSO and wet-season precipitation in the Arabian Peninsula. Journal of Climate, 28(12), 4743–4752. https://doi.org/10.1175/JCLI-D-14-00388.1

Kwarteng, A. Y., Dorvlo, A. S., & Vijaya Kumar, G. T. (2009). Analysis of a 27-year rainfall data (1977-2003) in the Sultanate of Oman. International Journal of Climatology, 29(4), 605–617. https://doi.org/10.1002/joc.1727

Lee, S., L'Heureux, M., Wittenberg, A. T., Seager, R., O'Gorman, P. A., & Johnson, N. C. (2022). On the future zonal contrasts of equatorial Pacific climate: Perspectives from

642 Observations, Simulations, and Theories. Npj Climate and Atmospheric Science 2022 5:1, 5(1),
643 1–15. https://doi.org/10.1038/s41612-022-00301-2
644
645 Mantua, N. J., Hare, S. R., Zhang, Y., Wallace, J. M., & Francis, R. C. (1997). A Pacific
646 Interdecadal Climate Oscillation with Impacts on Salmon Production. Bulletin of the American
647 Meteorological Society, 78(6), 1069–1079. https://doi.org/10.1175/1520-
648 0477(1997)078<1069:APICOW>2.0.CO;2
649
650 Matsuura, K., & Willmott, C. (2018, August). Terrestrial Precipitation: 1900-2017 Gridded
651 Monthly Time Series. Retrieved from
652 http://climate.geog.udel.edu/~climate/html_pages/Global2017/README.GlobalTsP2017.html
653
654 Mehmood, S., Ashfaq, M., Kapnick, S., Gosh, S., Abid, M. A., Kucharski, F., et al. (2022).
655 Dominant controls of cold-season precipitation variability over the high mountains of Asia. Npj
656 Climate and Atmospheric Science 2022 5:1, 5(1), 1–13. https://doi.org/10.1038/s41612-022-
657 00282-2
658
659 Patlakas, P., Stathopoulos, C., Flocas, H., Bartsotas, N. S., & Kallos, G. (2021). Precipitation
660 Climatology for the Arid Region of the Arabian Peninsula—Variability, Trends and Extremes.
661 Climate 2021, Vol. 9, Page 103, 9(7), 103. https://doi.org/10.3390/CLI9070103
662

663 Saeed, S., & Almazroui, M. (2019). Impacts of mid-latitude circulation on winter precipitation
664 over the Arabian Peninsula. Climate Dynamics, 53(9–10), 5253–5264.
665 https://doi.org/10.1007/s00382-019-04862-6
666
667 Saji, N. H., Goswami, B. N., Vinayachandran, P. N., & Yamagata, T. (1999). A dipole mode in
668 the tropical Indian ocean. Nature, 401(6751), 360–363. https://doi.org/10.1038/43854
669
670 Schnieder, U., Becker, A., Finger, P., Rustemeier, E., & Ziese, M. (2020). GPCC Full Data
671 Monthly Product Version 2020 at 0.25°: Monthly Land-Surface Precipitation from Rain-Gauges
672 built on GTS-based and Historical Data. .
673 https://doi.org/http://doi.org/10.5676/DWD_GPCC/FD_M_V2020_025
674
675 Syed, F. S., Adnan, S., Zamreeq, A., & Ghulam, A. (2022). Identification of droughts over Saudi
676 Arabia and global teleconnections. Natural Hazards, 112(3), 2717–2737.
677 https://doi.org/10.1007/s11069-022-05285-z
678
679 Zittis, G. (2017). Observed rainfall trends and precipitation uncertainty in the vicinity of the
680 Mediterranean, Middle East and North Africa. Theoretical and Applied Climatology 2017 134:3,
681 134(3), 1207–1230. https://doi.org/10.1007/S00704-017-2333-0